Radio Science

RESEARCH ARTICLE
10.1029/2023RS007726

High Performance Antenna System in MIMO Configuration for 5G Wireless Communications Over Sub-6 GHz Spectrum

Iftikhar ud Din[1], Mohammad Alibakhshikenari[2], Bal S. Virdee[3], Sadiq Ullah[1], Shakir Ullah[1], Muhammad Rizwan Akram[4], Syed Mansoor Ali[5], Patrizia Livreri[6], and Ernesto Limiti[7]

[1]Telecommunication Engineering Department, University of Engineering and Technology, Mardan, Pakistan, [2]Department of Signal Theory and Communications, Universidad Carlos III de Madrid, Madrid, Spain, [3]Center for Communications Technology, London Metropolitan University, London, UK, [4]Department of Electronic Engineering, Shanghai Jiao Tong University, Shanghai, China, [5]Department of Physics and Astronomy, College of Science, King Saud University, Riyadh, Saudi Arabia, [6]Department of Engineering, University of Palermo, Palermo, Italy, [7]Electronic Engineering Department, University of Rome "Tor Vergata", Rome, Italy

Key Points:

- A four elements multiple input and multiple output (MIMO) antenna systems operating at sub-6 GHz with ECC <0.1 and diversity >9.9 is presented for 5G communication
- A high isolation below −20 dB is achieved without the use of any decoupling network
- The MIMO system with dimension of 50Ã—50Ã—0.8 mm^3 has 41% fractional bandwidth and gain of 4.8 dBi

Correspondence to:
M. Alibakhshikenari,
mohammad.alibakhshikenari@uc3m.es

Citation:
Din, I., Alibakhshikenari, M., Virdee, B. S., Ullah, S., Ullah, S., Akram, M. R., et al. (2023). High performance antenna system in MIMO configuration for 5G wireless communications over sub-6 GHz spectrum. *Radio Science*, *58*, e2023RS007726. https://doi.org/10.1029/2023RS007726

Received 6 APR 2023
Accepted 14 SEP 2023

Author Contributions:
Conceptualization: Mohammad Alibakhshikenari, Sadiq Ullah, Muhammad Rizwan Akram, Patrizia Livreri, Ernesto Limiti
Data curation: Shakir Ullah
Formal analysis: Iftikhar ud Din, Sadiq Ullah, Shakir Ullah, Syed Mansoor Ali
Funding acquisition: Mohammad Alibakhshikenari
Investigation: Mohammad Alibakhshikenari, Bal S. Virdee, Muhammad Rizwan Akram, Syed Mansoor Ali
Methodology: Shakir Ullah, Syed Mansoor Ali
Project Administration: Mohammad Alibakhshikenari, Patrizia Livreri, Ernesto Limiti
Resources: Mohammad Alibakhshikenari

Abstract This paper presents a high-performance multiple input and multiple output (MIMO) antenna comprising 2 × 2 configuration of radiating elements that is designed for sub-6 GHz applications. The proposed MIMO antenna employs four identical radiating elements. High isolation between the radiating elements and therefore reduced mutual coupling is achieved by spatially arranging the radiating elements in an orthogonal configuration. Also, a novel frequency selective surface (FSS) was employed to increase the gain of the MIMO antenna over a wide bandwidth from 3 to 6 GHz. This was achieved by locating the FSS above the antenna at a certain height. The FSS essentially enhanced the antenna's directivity, reduced back lobe radiation and mutual coupling. The antenna was fabricated on a standard Rogers RT Duroid 5880 dielectric substrate with a 0.8 mm thickness. The overall dimension of the MIMO antenna is 50 × 50 × 12.5 mm^3 and it operates from 3.8 to 6 GHz, which corresponds to a fractional bandwidth of 41%. The proposed MIMO antenna has a measured peak gain of 4.8 dBi and inter radiation element isolation >20 dB. Its envelope correlation coefficient is <0.1 and diversity gain >9.9 (dB). These characteristics make the proposed MIMO antenna system suitable for 5G communication systems.

1. Introduction

Recent advancement in 5G wireless communication technology supports many data-driven wireless applications, seamless device-to-device connectivity, and the industrial revolution 4.0 (Gupta & Jha, 2015). Currently 5G communication has sufficient transmission capacity to provide reliable connectivity to numerous devices and this is done at relatively low power. This technology is enabling the advent of driverless vehicles, smart cities, and virtual reality (Rappaport et al., 2013). Future wireless technologies will benefit from 5G technology's promise to modernize the Internet of Things and expand the range of wireless communication (Hussain et al., 2019).5G band in the US from 3.8 to 4.2 GHz; in Japan from 3.8 to 4.2 GHz and 4.4–4.9 GHz; in China 4.4–4.5 GHz and 4.8–4.9 GHz. WLAN IEEE 802.11a/h/j/n/ac covers a frequency range from 5 to 5.8 GHz. As demand for wireless communication continues to grow rapidly, there is a need for additional spectrum resources to accommodate the increasing data requirements of modern applications. Hence, Federal Communications Commission (FCC) is planning to auction 5G frequency bands at 24, 28, 37, 39, and 47 GHz. These frequency bands represent underutilized or previously unallocated spectrum resources that can be utilized for 5G networks. Because of the widespread availability of commercially available wireless technology, the most recent innovation in telecommunications makes use of current base stations operating in the 3.5 and 4.5 GHz frequency bands (Desai, Upadhyaya, et al., 2020; Hussain et al., 2019; Saxena et al., 2018). In addition, wideband technology provides high throughput at a low cost in terms of both power consumption and price (Fathima et al., 2017). High throughput adaptability and integration improve electromagnetic testing, radar imaging, short-range radar, surveillance devices, medical imaging, and more (Madhav et al., 2019). Due to advances in technology and the connection of small devices, 5G systems must include a radiating element. As 5G develops rapidly, there is a need for hardware-dependent platforms that suit user needs (Arpan et al., 2020; Desai, Bui, et al., 2020) such as orbital angular momentum communications (Akram, Bai, et al., 2019; Akram, Mehmood, et al., 2019; Ove & Johansson et al., 2011), reconfigurable intelligent surfaces (Basar et al., 2019; El Mossallamy et al., 2020); and waveform selective antennas (Ushikoshi et al., 2023). For reliable wireless communication, single input single

Software: Iftikhar ud Din, Shakir Ullah, Muhammad Rizwan Akram
Supervision: Mohammad Alibakhshikenari, Ernesto Limiti
Validation: Mohammad Alibakhshikenari, Bal S. Virdee, Sadiq Ullah, Muhammad Rizwan Akram, Patrizia Livreri, Ernesto Limiti
Visualization: Iftikhar ud Din, Mohammad Alibakhshikenari, Bal S. Virdee, Sadiq Ullah, Patrizia Livreri
Writing – original draft: Iftikhar ud Din, Sadiq Ullah, Shakir Ullah
Writing – review & editing: Mohammad Alibakhshikenari, Bal S. Virdee, Syed Mansoor Ali, Patrizia Livreri, Ernesto Limiti

output (SISO) is not efficient. Hence, 5G systems use multiple input and multiple output (MIMO) technology to improve channel capacity and overcome multi-path fading (Madhav et al., 2019; Venkateswara Rao et al., 2019). The design of the MIMO system requires many radiating elements closely arranged on the same substrate and operating at the same frequency. MIMO antenna has a unique characteristic, that is, spatial multiplexing, which improves channel capacity and enables many users to communicate simultaneously in the same frequency band. MIMO is superior to SISO in terms of enhanced data throughput, high signal-to-noise ratio, improved efficiency, enhanced channel and multi-path fading (Biswas & Chakraborty, 2019; Roy et al., 2019). A typical MIMO antenna with four radiating elements has dimensions of 75×75 mm^2 and operates across 4.4–6.4 GHz (Chouhan & Malviya, 2020). The challenging criteria for the MIMO system are to design an antenna array that has very low mutual coupling amongst the MIMO radiating elements (Kundu, 2016) and able to fit in a limited space. So, when many radiating elements are positioned near each other, the electric field created by one antenna changes the surface currents of the adjacent antennas, consequently, the radiation characteristics and input impedance of each MIMO antenna deviate from its desired response (Qian, Huang et al., 2018). The influence of mutual coupling harshly reduces how the MIMO antenna element radiates, because of that, all the radiating elements must be carefully designed to minimize the mutual coupling. To minimize the space and mutual coupling amongst the MIMO elements, several techniques have been introduced that include the use of defected ground structures (Iqbal et al., 2017; Luo et al., 2015), neutral lines adjustment (Lee et al., 2009), and metamaterial inspired designs (Dabas et al., 2018; Farahani et al., 2010) to name a few. A wideband shared radiator having a size of 75×75 mm^2 with four-port excitation is reported in (Malviya & Chouhan, 2019). Another MIMO antenna having dimensions of 52×77.5 mm^2 and isolation of 15 dB is reported in (Deng et al., 2017). Furthermore, the MIMO system reported in (Dong et al., 2017; Jehangir et al., 2018; Lin et al., 2019; Shoaib et al., 2014) that operates at a frequency below 2 GHz has a relatively large size. In (Sharma & Wang, 2018) a unique tablet shape antenna was proposed and has a relatively large ground-plane and a bandwidth of 0.98 GHz from 1.71 to 2.69 GHz. Another design based on a four-port MIMO for WLAN application operating at 5.6–5.8 GHz is reported in (Aw et al., 2019; Khan et al., 2021; Pandit et al., 2018) that exhibits a wide bandwidth and has dimensions of 55×20 mm^2 with a gain of 2.4 dB. The above-mentioned MIMO antennas are relatively large and have low gain performance.

In this paper a high-performance MIMO antenna system comprising four radiation elements is designed and realized for sub-6 GHz applications. The current work is an extension of our previous paper (Din, Kiyani, et al., 2022). The antenna is constructed from four ring-shaped radiating elements designed to operate over a wide bandwidth from 4.2 to 6 GHz. The radiation elements in the proposed MIMO antenna system are oriented orthogonally relative to each other to enhance isolation between the radiators that otherwise would degrade the radiation characteristics of the MIMO antenna. The consequence of this type of arrangement to reduce mutual electromagnetic coupling is high radiation gain, wide bandwidth, excellent diversity gain (DG) and envelope correlation coefficient (ECC). Moreover, it is shown here that by locating the proposed frequency selective surface (FCC) above the antenna at a certain height the gain of the antenna is increased over a wide frequency range. These characterizing features make the proposed MIMO antenna system suitable for 5G applications.

2. Proposed Antenna Design

The investigation of the proposed 2×2 MIMO antenna system consisted of three stages. Firstly, a suitable radiating element was determined. The radiating element was then used in the design of a 2×1 antenna array. The configuration of the array was investigated to increase the isolation between the radiating elements. Finally, based on the results of the 2×1 antenna array, the proposed 2×2 MIMO antenna system was designed.

2.1. Design of Single Element Antenna

Inset in Figure 1 show a standard edged excited circular patch antenna and the proposed circular ring antenna. Both antennas have identical dimensions and are fabricated on identical dielectric substrate, that is, Rogers RT Duroid 5880 dielectric substrate with a 0.8 mm thickness. The size of both antennas is 25×25 mm^2. It can be observed from Figure 1 that the impedance match for $|S_{11}| \leq -10$ dB between 4 and 6 GHz is improved by hollow-

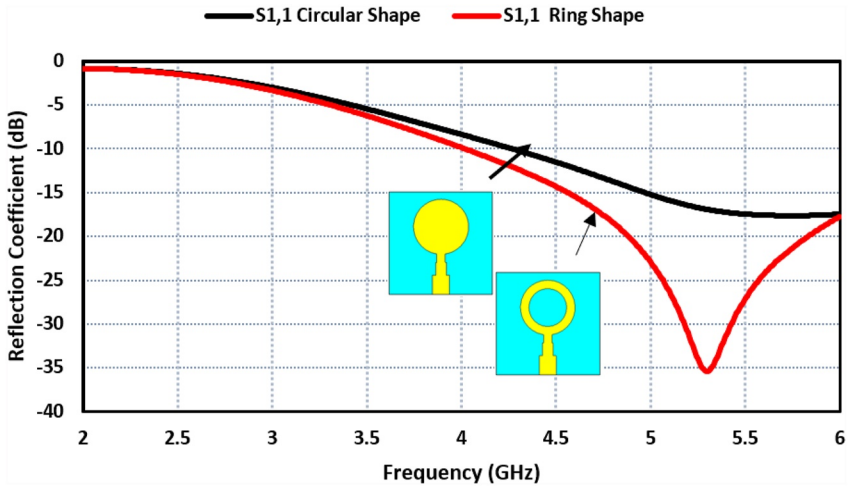

Figure 1. Reflection coefficient response of the circular shape radiator and the circular ring radiator.

ing the circular patch antenna. Figure 2 shows the circular ring patch antenna used in the proposed 2 × 2 MIMO antenna system. The ground-plane is truncated on the back side of the substrate and a rectangular shaped slot is embedded in the ground-plane. This modification enables the antenna to operate across a wideband necessary for sub-6 GHz 5G applications. The effective radius (R_e) of the circular patch antenna was determined using the following equation (Din, Ullah, al., 2022)

$$R_e = \left\{ \sqrt{1 + \frac{2H}{\pi \varepsilon_r R}\left(ln\frac{\pi R}{2H} + 1.7726\right)} \right\} \tag{1}$$

where H is the height of substrate, ε_r is the relative permittivity, and R is the radius of the antenna which is calculated using Equation 2 (Din, Ullah, et al., 2022). The dimensions of the antenna are listed in Table 1.

$$R \frac{F}{\left\{ \sqrt{1 + \frac{2h}{\pi \varepsilon_r F}\left(ln\frac{\pi F}{2H} + 1.7726\right)} \right\}} \tag{2}$$

where F is given by

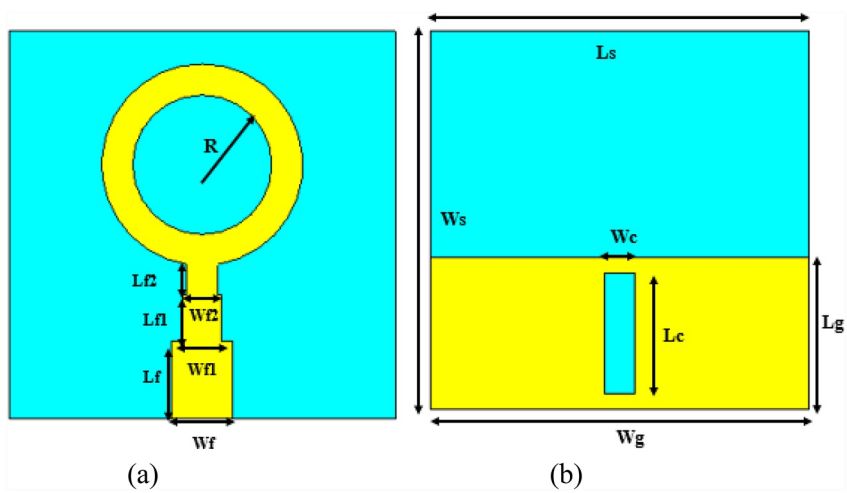

Figure 2. (a) Front view of the circular ring radiating element, and (b) Back view of the circular ring radiating element.

Table 1
Dimensions of the Circular Ring Antenna With Ground-Plane Slot

Parameters	Values (mm)	Parameters	Values (mm)	Parameters	Values (mm)
Ws	25	Wf	4	Ls2	50
Ls	25	Wf1	2.5	Ws1	50
Wg	25	Wf2	1.5	Ws2	50
Lg	10	R	4.5	Lf1	4
Lf	6	Lc	8	Wc	2
Lf2	4	Ls1	25	Wus	10
Lus	10	Lms	50	Wms	50
R1	4.7	H	15		

$$F = \frac{8.79 \times 10^9}{f_r \sqrt{\varepsilon_r}} \quad (3)$$

2.2. Antenna Evolution

The steps taken to design the circular ring antenna with truncated ground-plane slot are shown in Figure 3. In the first step the outer radius of the circular ring is determined from Equation 1. The ground-plane is truncated to the point where the feed line is connected to the patch antenna, as shown in Figure 3a. In the next step, the width of the microstrip feed is reduced at the neck of the circular ring patch. This is to improve the impedance matching characteristic between the feed line and the circular ring antenna. Also, a rectangular slot is cutout in the ground-plane under the feedline, as shown in Figure 3b. The feed line is tapered by including another step and the ground-plane slot is elongated,

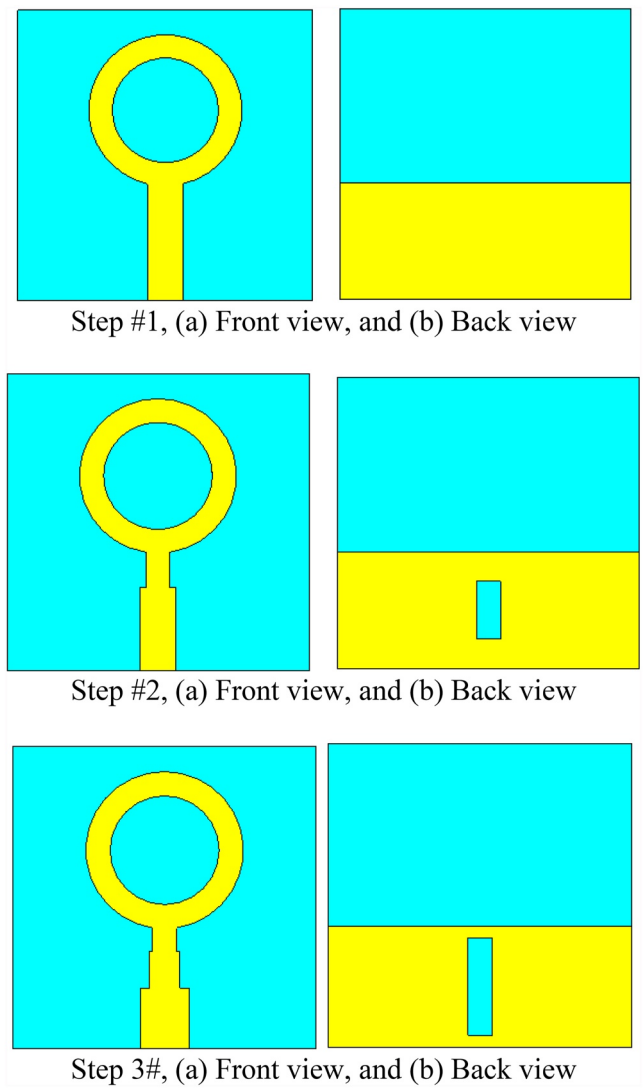

Figure 3. Design steps taken to realize the circular ring antenna with ground-plane slot.

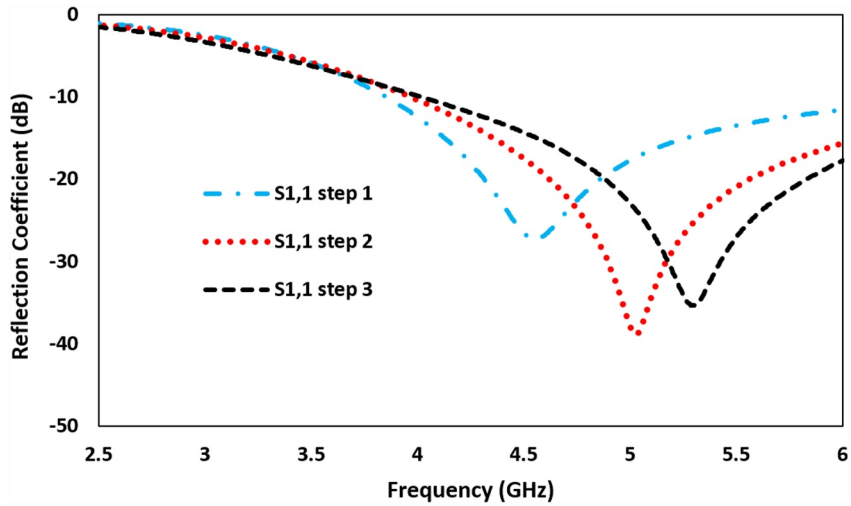

Figure 4. Reflection coefficient responses of design steps to realize the proposed circular ring antenna with ground-plane slot.

as shown in Figure 3c, to improve the impedance matching of the antenna for wideband performance. The reflection coefficient response corresponding to each step is shown in Figure 4. There are various reasons why ground-plane truncation improves the impedance matching. When a ground plane is present, it forms a capacitive coupling with the antenna structure. This capacitive coupling can lead to an impedance mismatch between the antenna and the feedline. By truncating or removing a portion of the ground plane, the capacitive coupling is reduced. This reduction in coupling helps in achieving a better impedance match with the feedline. The truncation of the ground plane also alters the current distribution on the antenna structure. The absence of a ground plane in certain areas changes the path of the currents, which can impact the impedance characteristics of the antenna. By carefully designing the truncation, it is possible to modify the current distribution in a way that improves the impedance matching with the feedline. Likewise, there are several reasons why the impedance match is improved with the ground-plane slot in a patch antenna. The presence of a ground-plane slot effectively increases the effective size of the patch antenna. This increased size allows for a better match between the electromagnetic waves in free space and the waves on the patch antenna. As a result, the impedance matching between the feedline and the patch antenna is improved. The ground-plane slot modifies the current distribution on the patch antenna. It introduces additional currents and changes the path of the current flow. This alteration in the current distribution can lead to a better match with the feedline impedance. Patch antennas inherently have a capacitive coupling with the ground plane due to their structure. This coupling can cause a mismatch between the antenna and the feedline impedance. By introducing a ground-plane slot, the capacitive coupling is reduced, thereby improving the impedance match. The ground-plane slot can also increase the bandwidth of the patch antenna. The slot alters the resonance properties of the antenna, allowing it to operate over a wider range of frequencies. A broader bandwidth can provide a better match to the feedline impedance over a wider frequency range.

2.3. Effect of Ground-Plane Slot on the Circular Ring Antenna

It's important to note that the design and placement of the ground-plane slot should be carefully optimized to achieve the desired impedance matching improvement. Various factors, such as the size, shape, and position of the slot, can influence its effectiveness.

The effect of the ground-plane slot on the antenna's reflection coefficient response therefore examined. Figure 5 shows how the slot length affected the reflection coefficient. It is observed from this figure the reflection coefficient at the resonance frequency of the antenna, that is, 5.3 GHz, has an optimum value of −48 dB for a slot length of 5.3 mm. For a shorter slot length of 4 mm the reflection coefficient is −40 dB, and for a larger slot length of

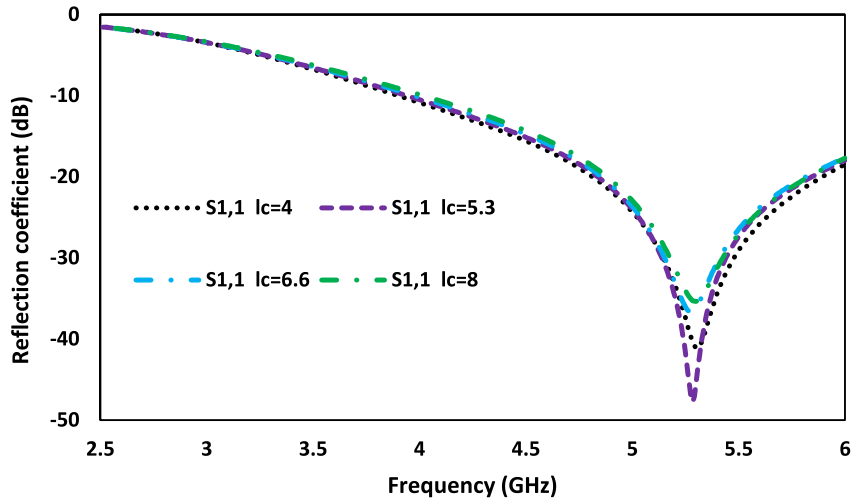

Figure 5. The effect on the reflection coefficient response of the circular ring antenna by the slot length. Unit is in millimeters.

8 mm the reflection coefficient is −37 dB. Figure 6 shows how the slot width affected the antenna's reflection coefficient performance. In this case the optimum reflection coefficient is −37 dB obtained at 5.4 GHz for a slot width of 1.6 mm. For a smaller width of 1 mm the reflection coefficient is −26.5 dB, and at a larger width of 3 mm the reflection coefficient degrades to −18 dB. Therefore, in the design the slot length and width chosen were 5.3 and 1.6 mm, respectively.

3. Two Element MIMO Antenna System

A two element MIMO antenna was realized by co-locating two identical circular ring antennas on a common dielectric substrate. The two radiating elements were arranged orthogonally as shown in Figure 7. The size of the 2×1 antenna array is 25×50 mm^2. The gap between the radiating elements is 12.5 mm, which is equivalent to $0.2\lambda_o$ at 5 GHz. The simulation results in Figure 8 show the isolation of the resulting MIMO antenna is greater than 20 dB over a wide bandwidth of 2.5 GHz from 2.5 to 6 GHz.

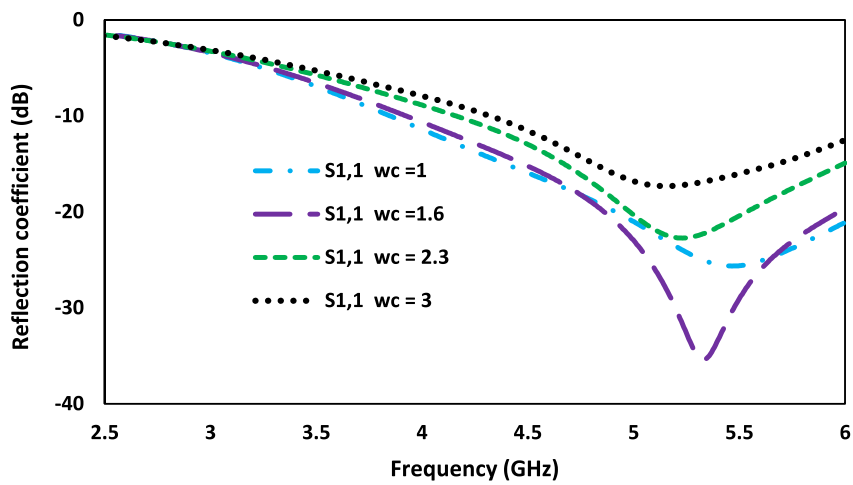

Figure 6. The effect on the reflection coefficient response of the circular ring antenna by the slot width. Unit is in millimeters.

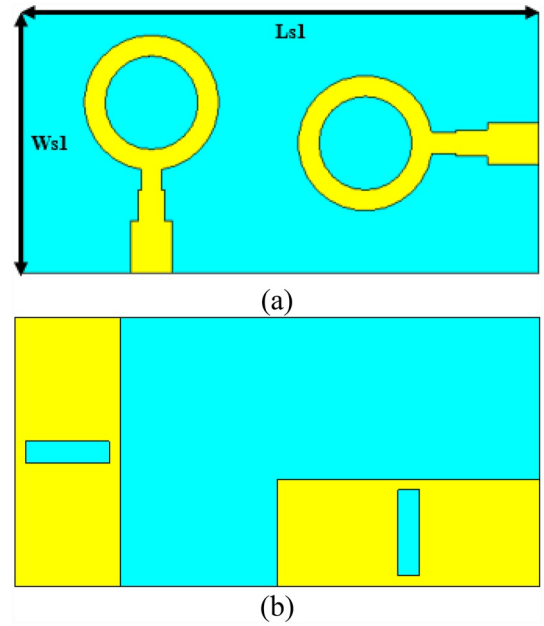

Figure 7. 2 × 1 element multiple input and multiple output configuration of the circular ring antenna with ground-plane slot, (a) top side, and (b) bottom side.

S-parameters of the fabricated 2 × 1 element prototype MIMO antenna, shown in Figure 9, was tested using Vector Network Analyzer and compared with the simulation results in Figure 10. The MIMO antenna has a measured impedance bandwidth of 2.2 GHz from 3.8 to 6 GHz. The discrepancy between the measured and simulated results is attributed to fabrication tolerance. It is possible to reduce the discrepancies and improve the accuracy of the antenna performance evaluation by iteratively refining the design, fabrication, simulation, and measurement processes.

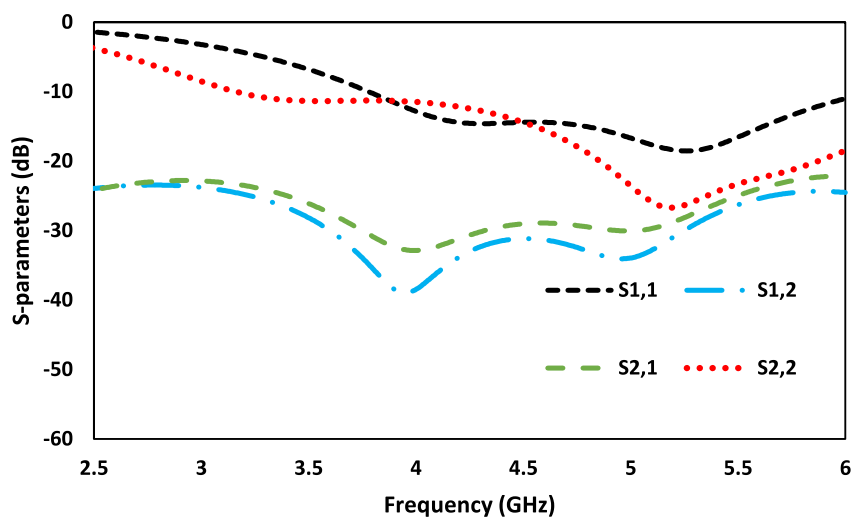

Figure 8. S-parameters of the 2 × 1 element multiple input and multiple output antenna.

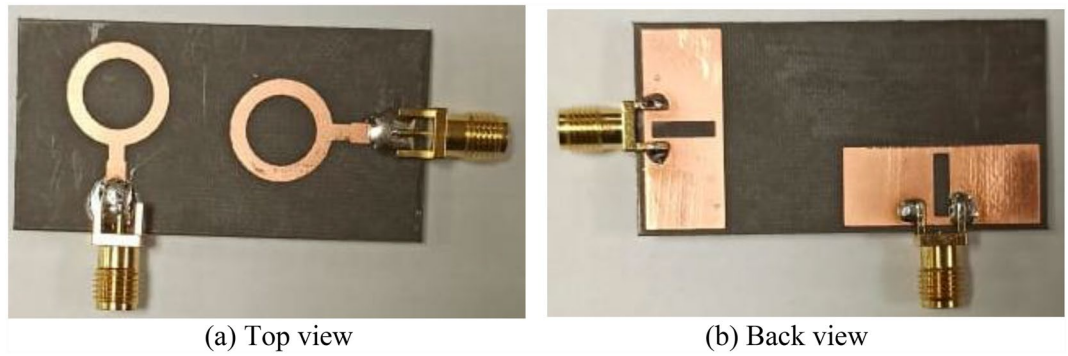

Figure 9. The fabricated 2 × 1 element multiple input and multiple output antenna.

4. Four Element MIMO Antenna System

A 2 × 2 element MIMO antenna design is based on the 2 × 1 element MIMO antenna, as shown in Figure 11. All four radiating elements are orthogonal with respect to each other. The antenna was fabricated on Rogers RT Duroid 5880 substrate and had an overall size of 50 × 50 mm^2.

The gap between the antennas is sufficient to prevent significant coupling that can otherwise degrade the radiation characteristics of the antenna array. The orthogonal arrangement ensures that the electric field vectors of the two waves are perpendicular to each other. This antenna arrangement ensures circular polarization because it enables the generation of two orthogonal linearly polarized waves, which, when combined, result in circular polarization. It's important to note that the phase and amplitude relationship between the two orthogonal antennas must be precisely controlled to achieve the desired circular polarization. Any deviations in the phase or amplitude balance can result in elliptical polarization rather than pure circular polarization. Therefore, careful design and calibration are necessary to ensure the proper orthogonal arrangement and achieve accurate circular polarization. The measured S-parameters of the proposed 2 × 2 element MIMO antenna are shown in Figure 12. The isolation between the radiating elements is greater than 20 dB and this is achieved without using any decoupling network.

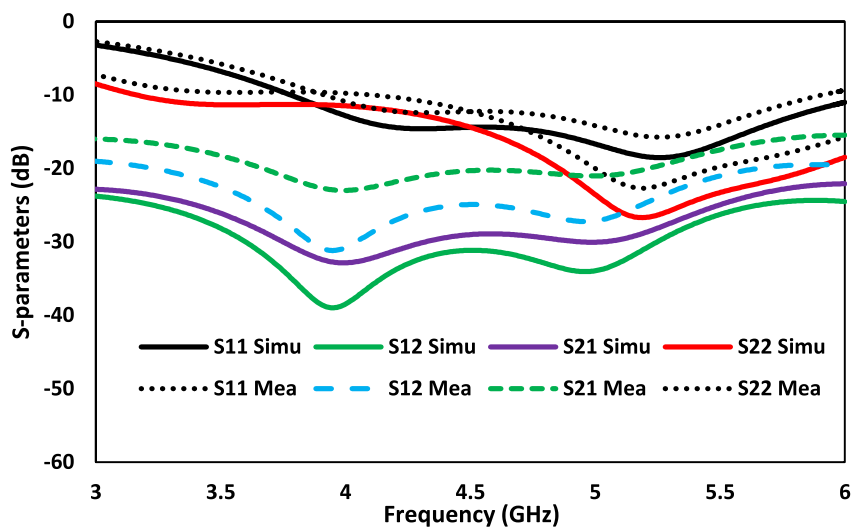

Figure 10. Simulated and measured S-parameters of the 2 × 1 element multiple input and multiple output antenna.

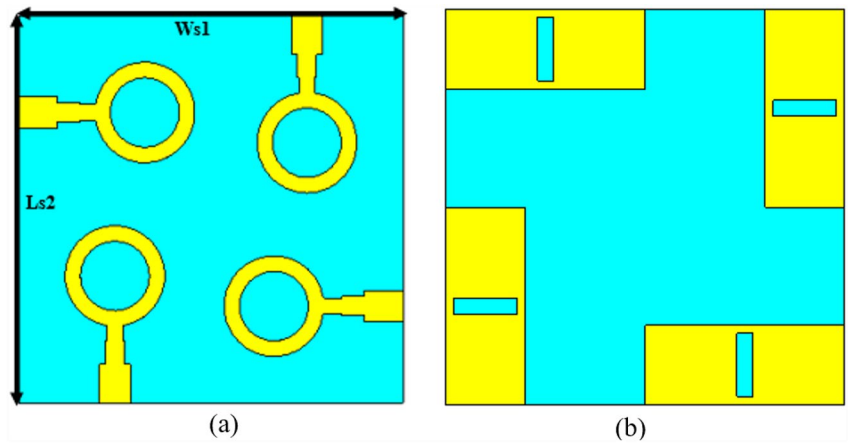

Figure 11. The proposed 2 × 2 element multiple input and multiple output antenna, (a) Front view, and (b) Back view.

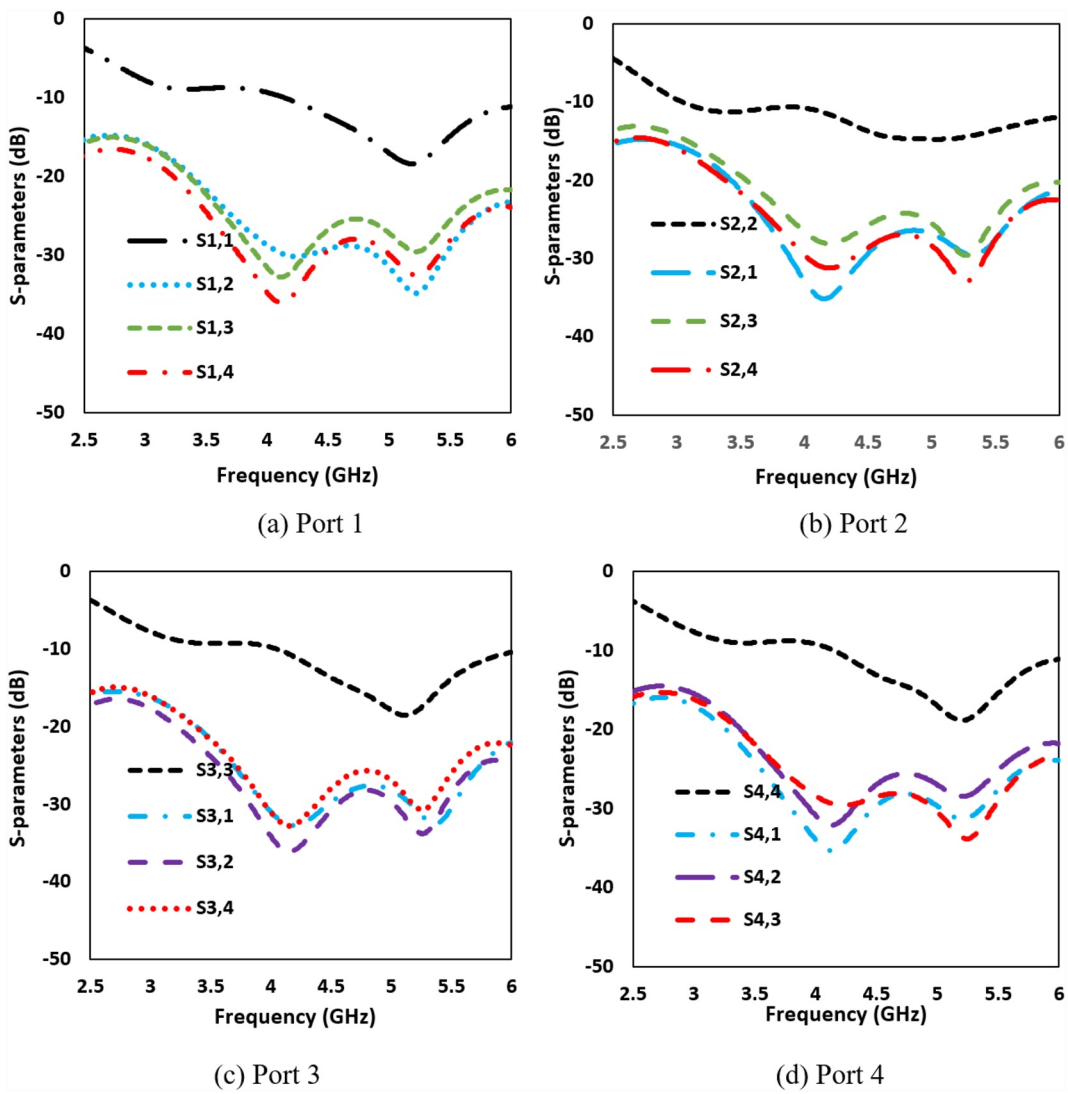

Figure 12. S-parameters at each port of the proposed 2 × 2 element multiple input and multiple output antenna.

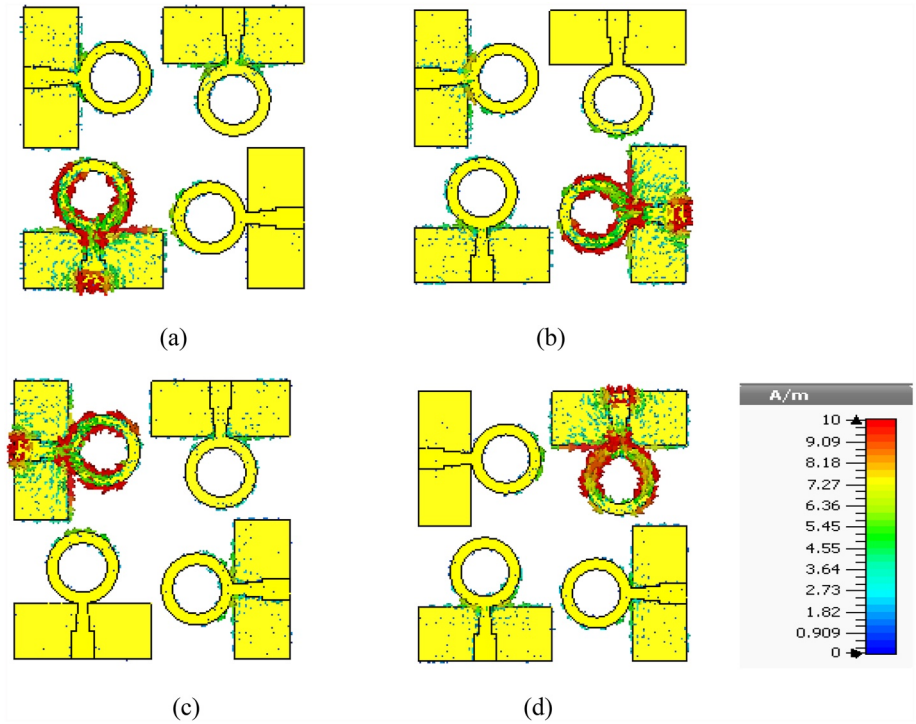

Figure 13. Surface current density distribution over the proposed 2 × 2 element multiple input and multiple output antenna at 4.5 GHz, (a) port 1, (b) port 2, (c) port 3, and (d) port 4.

5. Surface Current and Electric Field Distribution

The surface currents distribution over the proposed 2 × 2 element MIMO antenna is shown in Figure 13. It can be observed from this figure that the surface currents are mainly concentrated around the periphery of the circular ring antenna that is being excited. This is because at the edges of an antenna, there is a sudden change in the electrical properties of the surface. This change in boundary conditions causes a concentration of the surface current. The edges act as the transition region between the conducting antenna structure and the surrounding environment. The current tends to accumulate at the edges to satisfy the boundary conditions imposed by the surrounding medium. It is also noticeable that the surface currents over the other antennas are negligible indicating high isolation between the adjacent antennas due to minimal electromagnetic interactions.

Figure 14 shows the electric field intensity over the 2 × 2 element MIMO antenna at 4.5 GHz with the radiating elements are excited one at a time. The electric field is concentrated at the feedline and the periphery of the circu-

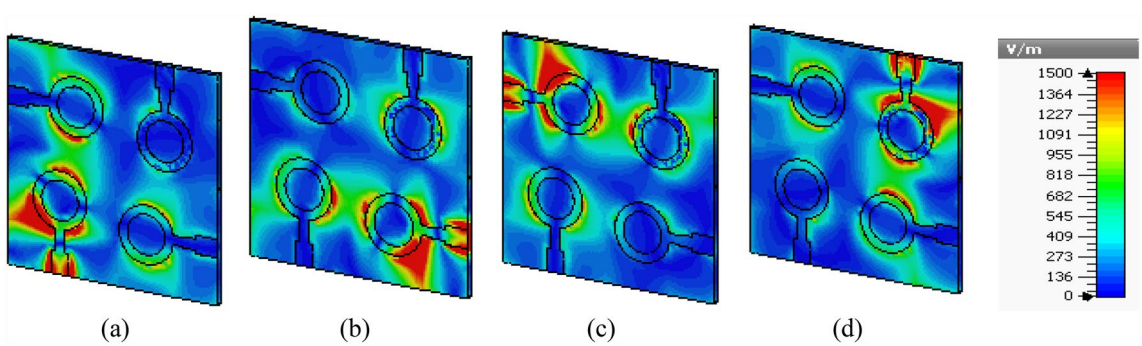

Figure 14. Electric field over the proposed multiple input and multiple output antenna at 4.5 GHz for (a) port 1 excitation, (b) port 2 excitation, (c) port 3 excitation, and (d) port 4 excitation.

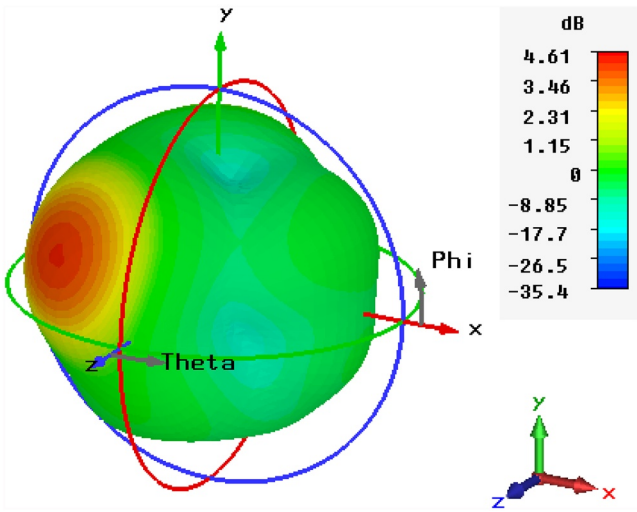

Figure 15. Simulated 3D radiation plot of the 2 × 2 element multiple input and multiple output antenna at 4.5 GHz.

lar ring antenna. In a circular ring antenna, the electric current flows along the circumference of the ring. As a result, the electric field is strongest where the current is concentrated. It can also be observed that the electromagnetic coupling between the antennas is minimal. This is due to the orthogonal arrangement of the radiating elements. The simulated 3D radiation plot of the MIMO antenna at 4.5 GHz is shown in Figure 15. The 2 × 2 element MIMO antenna is placed in the *xy*-plane.

6. Gain Enhancement of the Proposed MIMO Antenna

6.1. Frequency Selective Surface

Frequency selective surfaces (FSS) are engineered structures that exhibit different transmission or reflection properties at a defined frequency range. FSS is commonly used to transmit or block specific frequency bands (Din et al., 2023). The proposed FSS is employed here to improve the performance of the MIMO antenna by improving its impedance matching. The FSS unit cell used here was implemented on Rogers RT/Duroid 5880 substrate with a thickness of 0.8 mm. The design of the proposed unit cell involved creating a circular slot in a square patch, as illustrated in Figure 16a. The S-parameter responses of the square patch and the square patch with a circular slot are shown in Figure 16b. It is evident from this figure that the isolation of the square patch with a circular slot exhibits isolation much greater than 20 dB between 3 and 6 GHz, and a peak isolation of above 40 dB at 4.2 GHz.

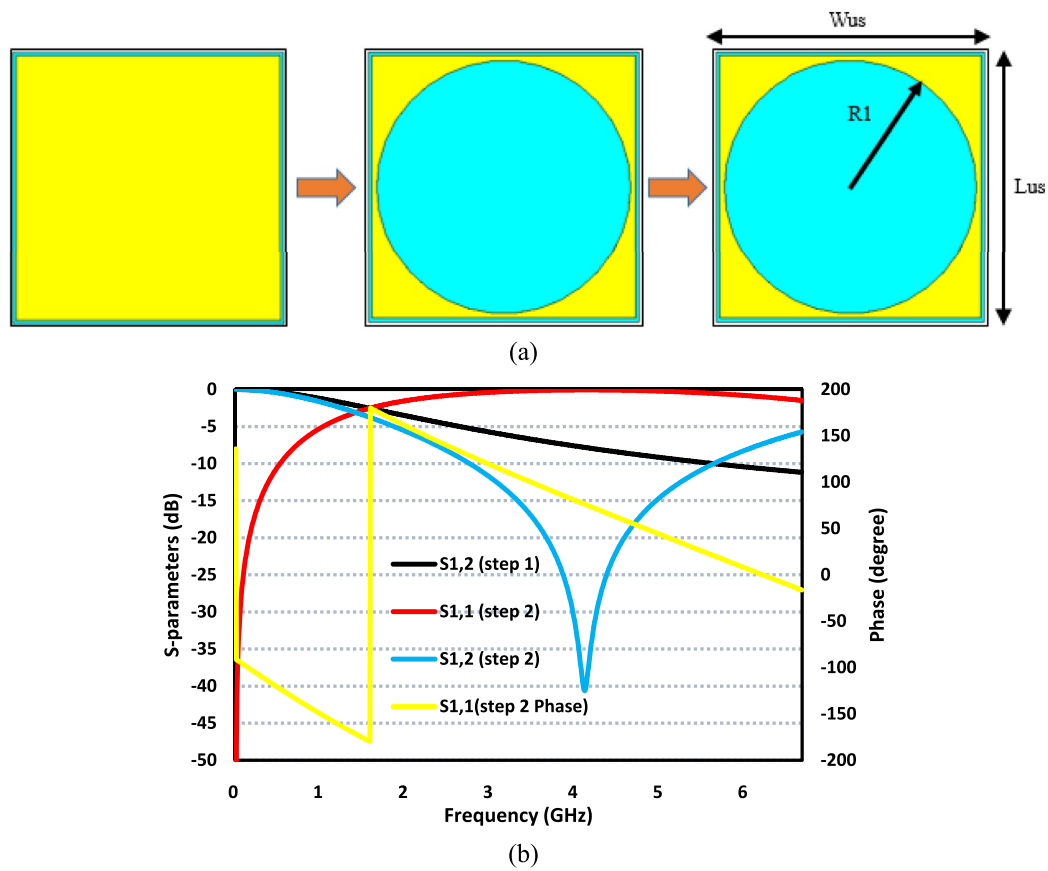

Figure 16. (a) Steps to create the unit cell, and (b) S-parameter response of the unit cell.

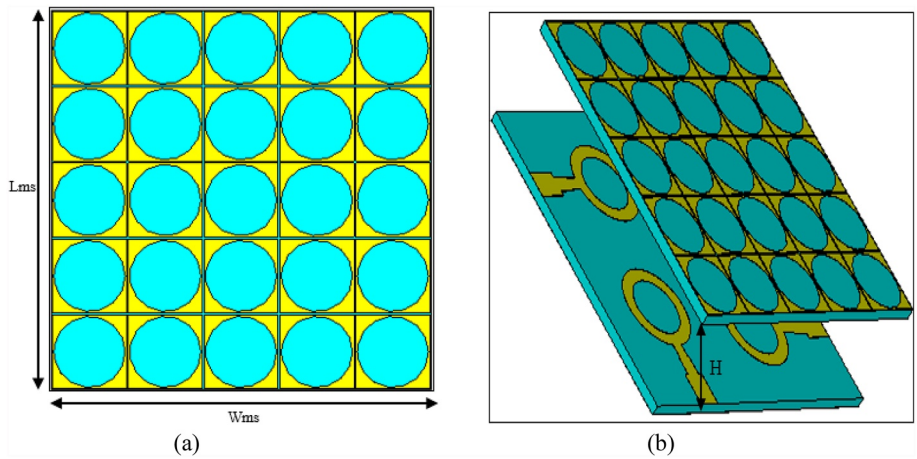

Figure 17. (a) Layout of the frequency selective surface (FSS), and (b) FSS based 2 × 2 multiple input and multiple output antenna array.

6.2. FSS Based MIMO Antenna

The layout of the FSS based MIMO antenna is shown in Figure 17. The proposed FSS of size 50 × 50 mm^2 consists of 25-unit cells positioned in 5 × 5 matrix. The FSS is located above the MIMO antenna at a height (H) to increase the MIMO antenna's gain. The improvement in antenna gain is due to enhanced directivity, back lobe reduction, and reduction in mutual coupling. The S-parameters of FSS based MIMO antenna are shown in Figure 18. The reflection coefficient of the MIMO antenna for $S_{11}| \leq -10$ dB at its four ports shown in Figure 18a extends between 3.2 and 6 GHz, corresponding to an impedance bandwidth of 2.8 GHz. Figure 18b shows the isolation between the four antennas is greater than 20 dB between 3.7 and 5.3 GHz, and greater than 14 dB across 3.5 and 6 GHz. The bandwidth enhancement is attributed to improvement in impedance matching.

6.3. Gap Affect Between the FSS and MIMO Antenna

The effect of the gap between FSS and the MIMO antenna on the gain performance is shown in Figure 19. The height was varied between 7.5 and 15 mm. The gain is greater than 2 dBi across 3 and 6 GHz however it is better than 5 dBi for a height of 10–15 mm between 3.75 and 5.6 GHz. A height of 12.5 mm provides an optimum gain better than 5 dB between 3.6 and 6 GHz. Figure 20 shows the proposed MIMO antenna with and without FSS. It is evident from this figure that by mounting the FSS above the MIMO antenna the gain is increased by an average of 1.5 dB. The gain is better than 6 dBi between 3.8 and 5 GHz.

7. Measured Results of the Proposed FSS Based MIMO Antenna Array

The proposed FSS based MIMO antenna array was fabricated, and its performance was measured in terms of radiation pattern and S-parameters using a Vector Network Analyzer. A photograph of the front and back of the fabricated antenna and the FSS structure are shown in Figure 21. The measured S-parameter of the FSS based MIMO antenna array is shown in Figure 22 when the four ports are excited individually. In all four cases, the isolation between the radiating elements is greater than 15 dB from 3.5 to 6 GHz.

The simulated and measured antenna gain of the 2 × 1 and 2 × 2 element FSS based MIMO antenna array is shown in Figure 23. The gain of the 2 × 1 element MIMO antenna varies between 2.2 dBi to a maximum of 4 dBi. Its average gain is approximately 3 dBi. In the case of the 2 × 2 element MIMO antenna the gain varies between 3i and 4.5 dBi, and it has an average gain of approximately 3.8 dBi.

The measured radiation pattern of the proposed 2 × 2 element FSS based MIMO antenna array in the E-plane and H-plane at 4.5 and 5.5 GHz are shown in Figure 24. A conventional measurement setup was used to

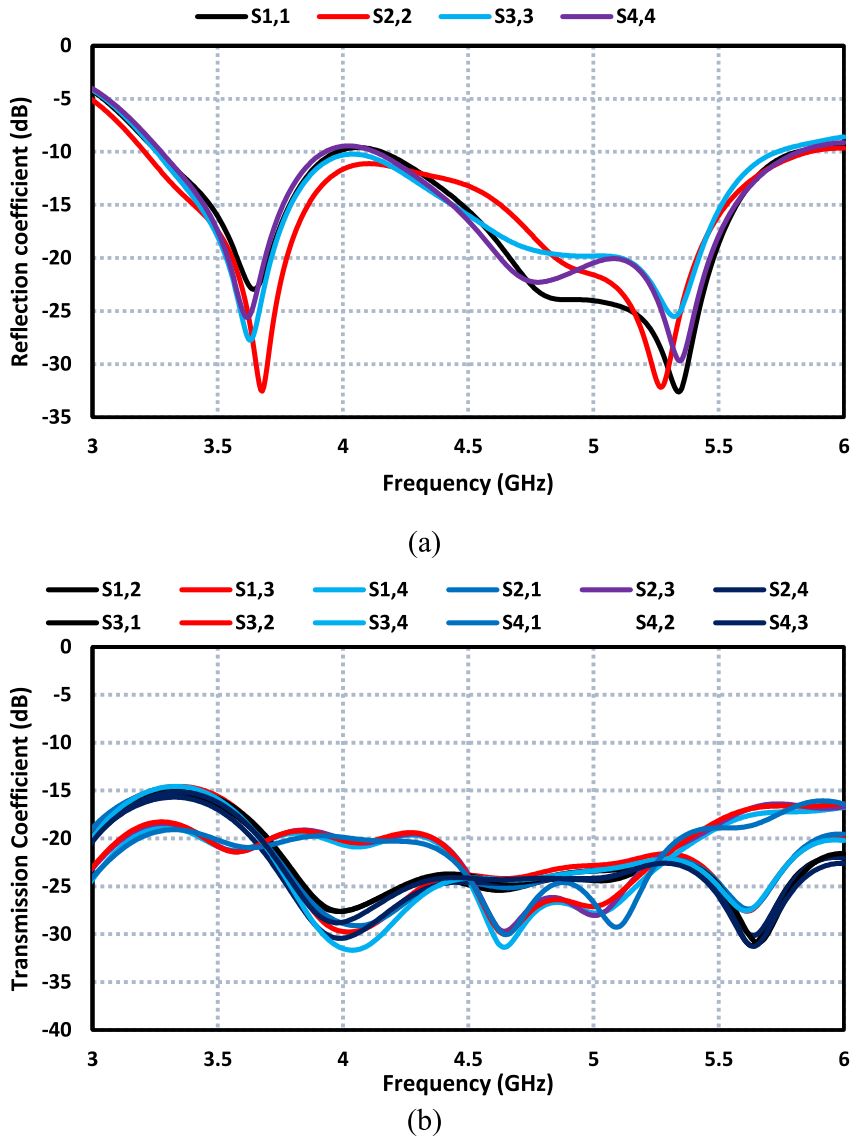

Figure 18. Frequency selective surface based multiple input and multiple output antenna array, (a) Reflection coefficient response, and (b) Transmission coefficient response.

measure the radiation patterns in an anechoic chamber. A calibrated reference antenna was used to establish a reference point for measurements and ensure accuracy. The far-field measurement in both principal planes was done over an angle from −180° to 180°. There is a good correlation between the simulated and measured results. The discrepancy in the results is attributed to inaccurate modeling and manufacturing tolerances. This is because the simulation is based on mathematical models and assumptions about the antenna's behavior and the surrounding environment. As these assumptions do not accurately reflect the real-world conditions, because of the presence of nearby objects or the effect of the antenna's mounting structure, the simulated results are likely to differ from the actual measurements. Also, the antenna is manufactured with certain tolerances, which can result in variations in their electrical and mechanical properties. These tolerances may not be fully accounted for in the simulation models, leading to discrepancies between the simulated and measured radiation patterns.

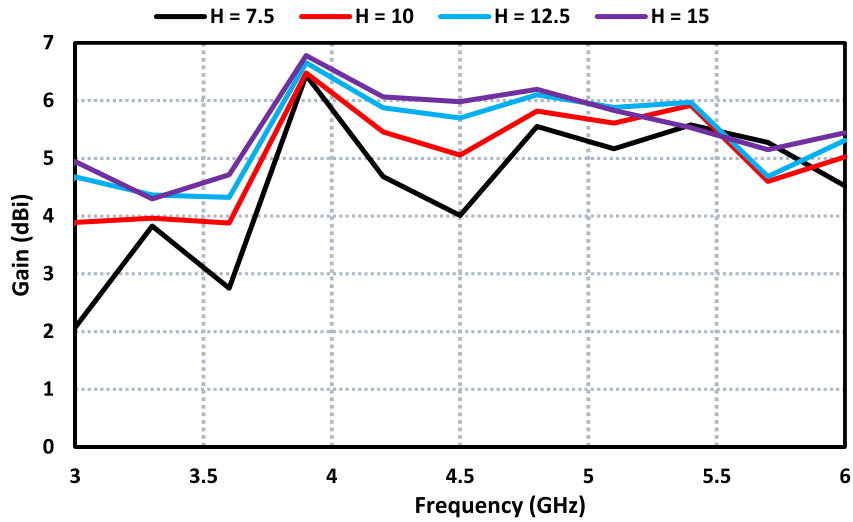

Figure 19. Simulated gain response of the 2 × 2 multiple input and multiple output (MIMO) antenna as a function of gap between the frequency selective surface and MIMO antenna. Units are in millimeters.

8. Diversity Parameters of the Proposed FSS Based MIMO Antenna

The ECC is a measure of the similarity between antenna ports in terms of their radiated signals. It quantifies the correlation or similarity of the envelopes of the signals, rather than the phase or magnitude of the signals themselves. ECC was calculated using Equation 4 (Malviya & Chouhan, 2019). Diversity gain (DG) refers to the improvement in the performance of a wireless communication system achieved by using multiple antennas. It is a measure of the antenna array's ability to combat fading, interference, and other impairments that can degrade the quality of the received signal. DG was calculated using Equation 5 (Malviya & Chouhan, 2019).

$$ECC = \frac{|S_{11}^{*}S_{12} + S_{21}^{*}S_{22}|^{2}}{\left(1 - \lfloor S_{12}\rfloor^{2} - \lfloor S_{22}\rfloor^{2}\right)\left(1 - \lfloor S_{22}\rfloor^{2} - \lfloor S_{12}\rfloor^{2}\right)} \tag{4}$$

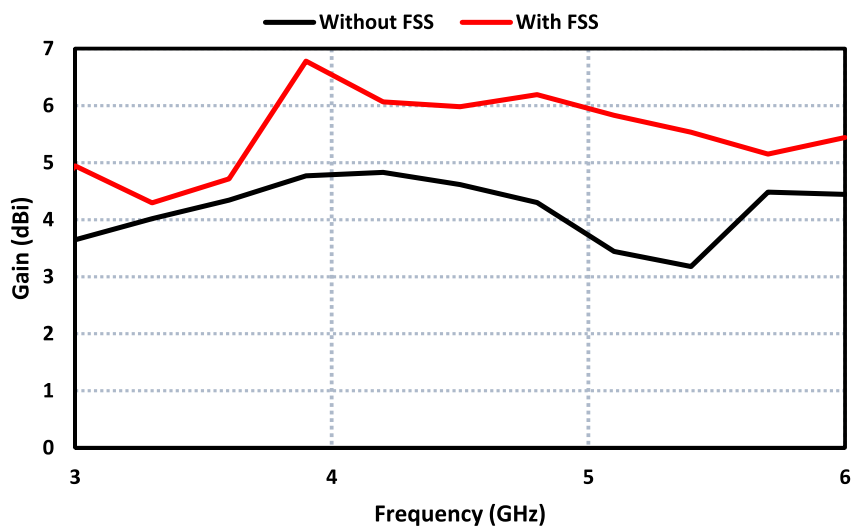

Figure 20. Simulated gain response of the 2 × 2 multiple input and multiple output antenna with and without frequency selective surface reflector.

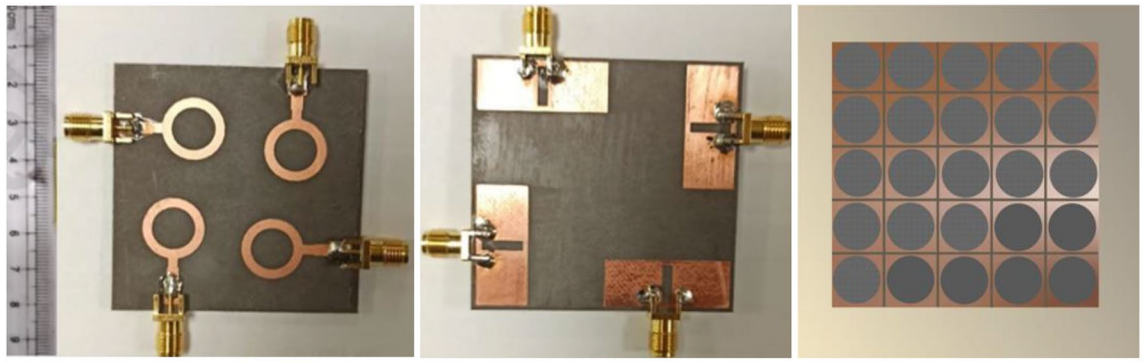

(a) (b) (c)

Figure 21. Fabricated prototype of the proposed frequency selective surface (FSS) based multiple input and multiple output antenna, (a) top view, (b) bottom view, and (c) FSS structure.

$$DG = 10 \times \sqrt{(1 - ECC)} \tag{5}$$

Ideally, ECC should be 0, but in real situations an acceptable value of ECC is below 0.5 (ECC < 0.5). The magnitude of ECC between the ports of the 2 × 2 element FSS based MIMO antenna array is shown in Figure 25. This figure shows the magnitude of the ECC to be less than 0.1.

Diversity gain on the order of 10 dB is highly desirable in wireless communication systems. A DG of 10 dB implies a tenfold improvement in the SNR or BER compared to a single-antenna/single-path system. Figure 26 shows the proposed 2 × 2 element FSS based MIMO antenna array has a DG of better than 9.5 dB. DG across the operational range 4–6 GHz is nearly 10 dB. This indicates that the proposed antenna array is effective in combating fading, interference, and other impairments, leading to improved signal quality, reliability, and overall system performance.

Channel capacity loss (CCL) refers to the reduction in the achievable data rate or capacity of a communication channel due to various factors and impairments. It quantifies the decrease in information-carrying capacity compared to the ideal theoretical limit set by the channel's bandwidth and signal-to-noise ratio. The CCL is measured in bits per second per Hertz (bits/sec/Hz) and its value must be less than 0.4. CCL can be calculated using the following expressions (Khalid et al., 2020).

$$\mathrm{CCL} = -\log_2 \det(a) \tag{6}$$

$$\mathrm{a} = \begin{bmatrix} \sigma_{11} & \sigma_{12} \\ \sigma_{21} & \sigma_{22} \end{bmatrix} \tag{7}$$

$$\sigma_{ii} = 1 - \left(|S_{ii}|^2 - |S_{ij}|^2\right) \tag{8}$$

$$\sigma_{ij} = -\left(S_{ii}{}^{*} S_{ij} + S_{ji} S_{jj}{}^{*}\right) \tag{9}$$

where σ_{ii} and σ_{ij} are the correlation coefficients between antenna ports ii and ij. Figure 27 shows the CCL of the 2 × 2 element FSS based MIMO antenna array is less than 0.4 between 3.1 and 6 GHz.

Another important parameter is mean effective gain (MEG). This parameter is used to characterize the average gain of an antenna in a specific direction. It provides an indication of the antenna's ability to concentrate radiated or received power in a particular direction. The magnitude of MEG must be in a range from −3 dB ≤ MEG ≤ −12 dB. It can be calculated using Equations 10 and 11 (Saadh et al., 2020). Figure 28 shows the MEG between the ports to be in the range −3 dB and −12 dB across 3.3 and 6 GHz.

$$\mathrm{MEG}_i = 0.5\left[1 - |S_{ii}|^2 - |S_{ij}|^2\right] \tag{10}$$

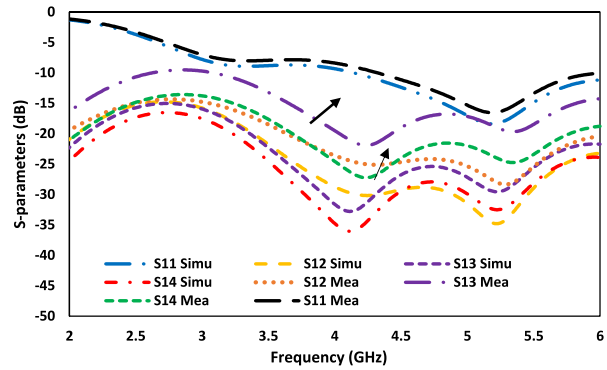

(a) Excitation - port 1

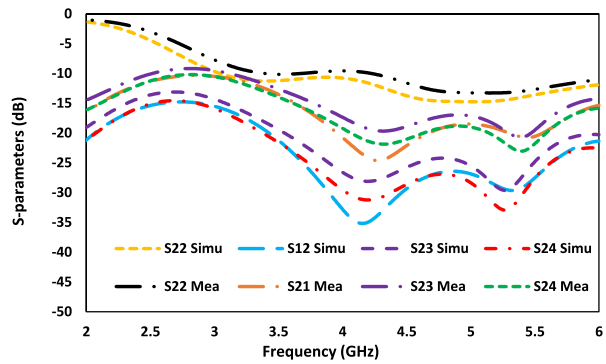

(b) Excitation - port 2

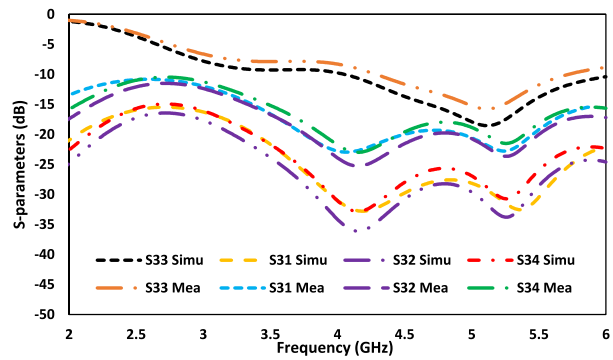

(c) Excitation - port 3

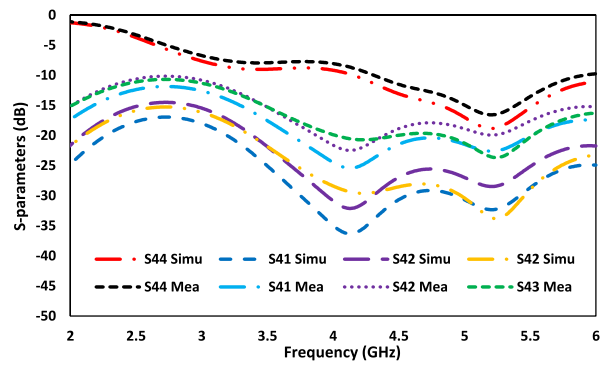

(d) Excitation - port 4

Figure 22. Measured and simulated S-parameters of the proposed frequency selective surface based multiple input and multiple output antenna array.

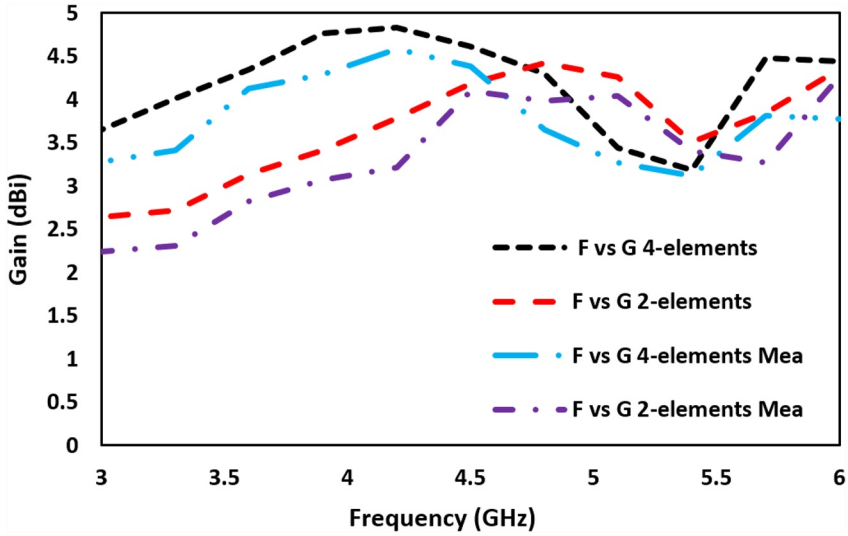

Figure 23. Measured and simulated gain of the 2 × 1 element and 2 × 2 element of the proposed multiple input and multiple output antenna array.

$$\mathrm{MEG}_j = 0.5\left[1 - |S_{ij}|^2 - |S_{jj}|^2\right] \tag{11}$$

Another important parameter is the total active reflection coefficient (TARC). This parameter is a measure used to assess the reflection of an electromagnetic wave at the interface between two media. It accounts for both the magnitude and phase of the reflected wave, considering the power that is reflected back toward the source. TARC for *N*-element MIMO antenna can be calculated using the following expression (Saadh et al., 2020).

$$\mathrm{TARC} = \frac{\sqrt{\Sigma_{i=1}^{N}|b_i|^2}}{\sqrt{\Sigma_{i=1}^{N}|a_i|^2}} \tag{12}$$

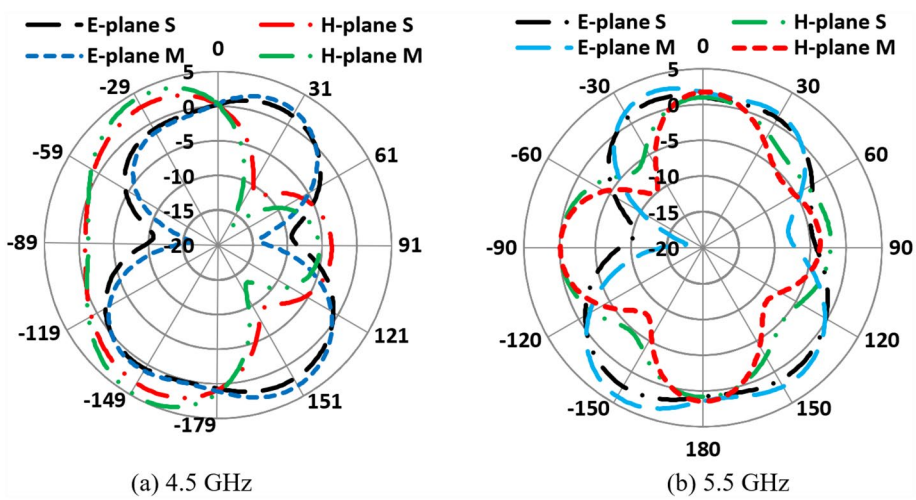

Figure 24. 2D plots of the 2 × 2 element frequency selective surface based multiple input and multiple output antenna array, (a) at 4.5 GHz, and (b) at 5.5 GHz.

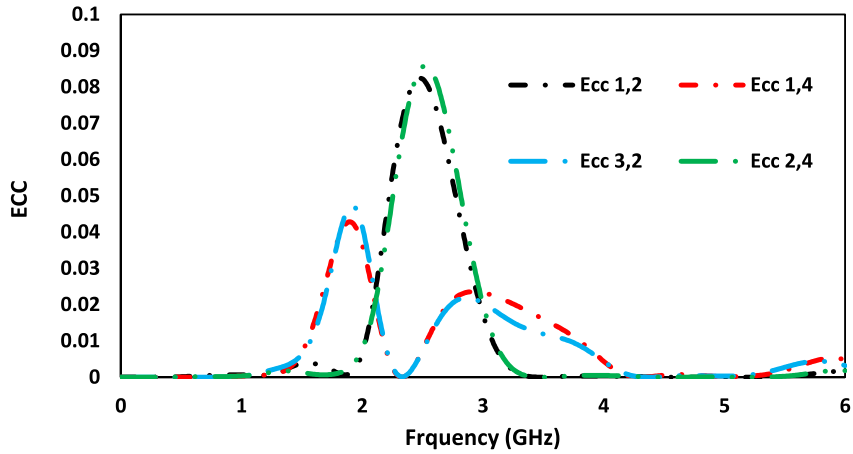

Figure 25. Envelope correlation coefficient of the proposed 2 × 2 element frequency selective surface based multiple input and multiple output antenna array.

Ideally, TARC should be zero which means all the power delivered is accepted by the FSS based MIMO antenna array and vice versa. However, in practical scenarios, it is challenging to achieve a TARC value of exactly zero due to various factors, including impedance mismatches, imperfect components, and reflections caused by impedance changes or structural features. The goal in many cases is to minimize the TARC to the greatest extent possible. The TARC for the proposed 2 × 2 element FSS based MIMO antenna array is shown in Figure 29. The TARC is better than −9 dB between 3 and 6 GHz.

The salient parameters of the proposed 2 × 2 element FSS based MIMO antenna array are compared with previous works in Table 2. Compared to 4-element radiators the proposed MIMO antenna exhibits the largest impedance bandwidth, however its peak gain is comparable to other 4-element MIMO antennas. Moreover, except for (Malviya & Chouhan, 2019) it has a relatively small surface area.

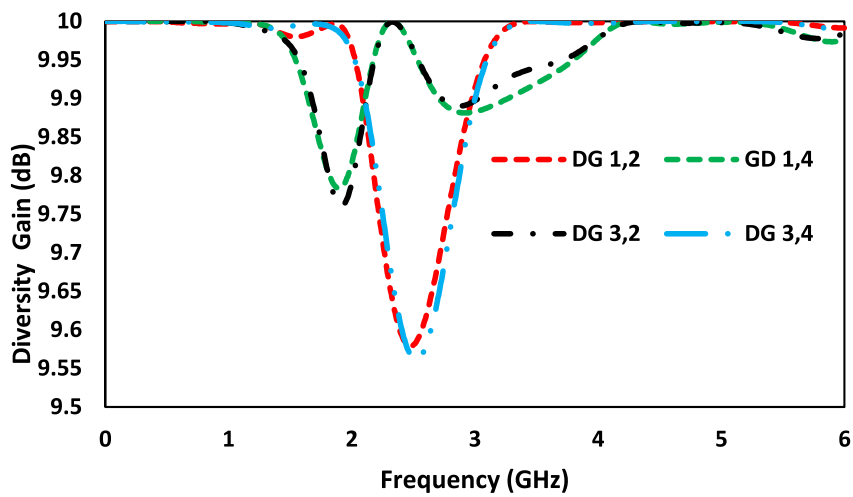

Figure 26. Diversity gain of the 2 × 2 element frequency selective surface based multiple input and multiple output antenna array.

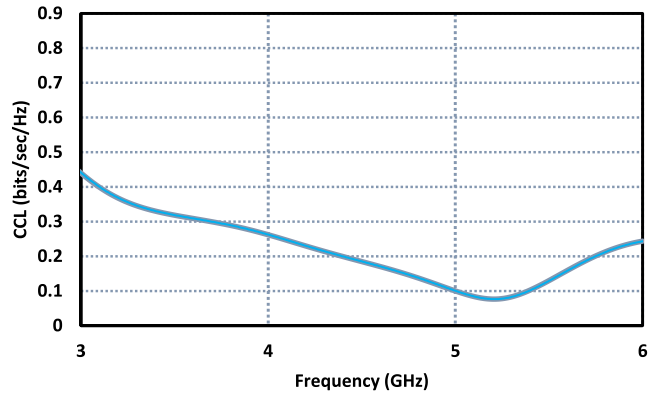

Figure 27. Channel capacity loss analysis of the presented frequency selective surface based multiple input and multiple output antenna array.

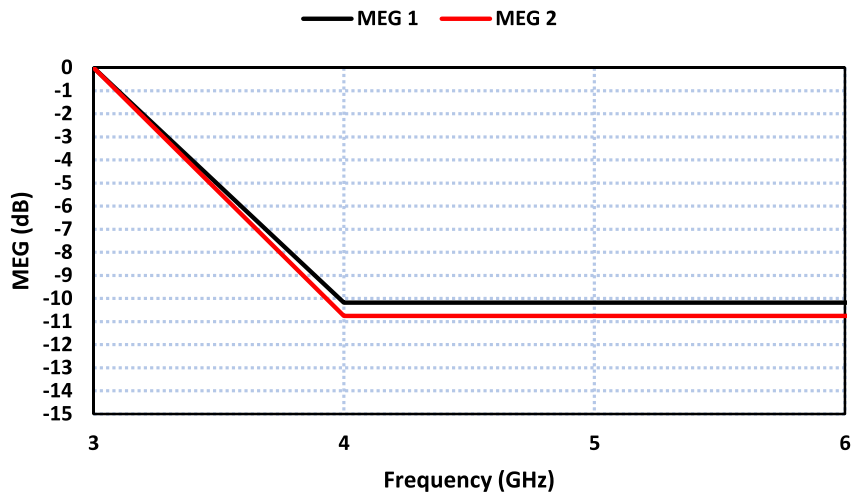

(a)

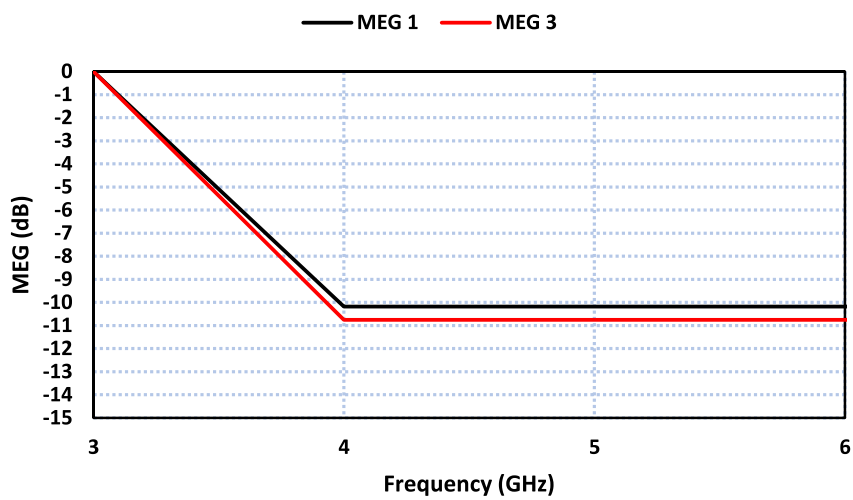

(b)

Figure 28. (a) mean effective gain (MEG) between ports 1 & 2, and (b) MEG between ports 1 & 3.

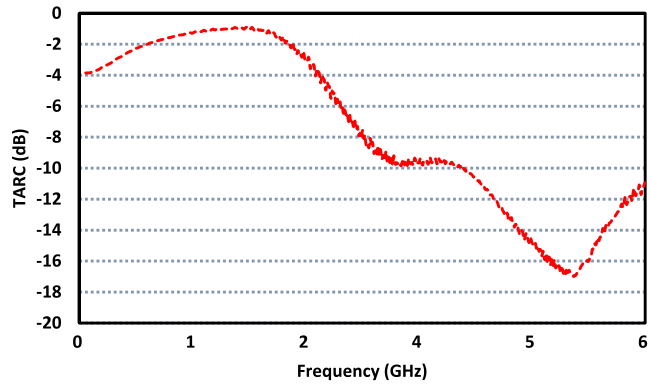

Figure 29. Total active reflection coefficient of the proposed 2 × 2 element frequency selective surface based multiple input and multiple output antenna array.

Table 2
Comparison With the Previous Works

Ref no.	Size (λ_o^2)	Freq. range/impedance bandwidth (GHz)	Peak gain (dBi)	No. of elements
(*Kundu et al.*, 2016)	1.2 × 1.2	4.96–5.50/0.54	5.5 @ 4.75 GHz	4
(*Qian et al.*, 2018)	0.43 × 0.3	2.4–2.48/0.08	-	2
		5.15–5.825/0.675		2
(*Farahani et al.*, 2010)	0.87 × 0.1	1.71–2.69/0.98	1 @ 1.7 GHz	2
(*Malviya et al.*, 2019)	0.48 × 0.48	5.6–5.8/0.2	1.8 @ 5.6 GHz	4
(*Deng et al.*, 2017)	1 × 0.4	4.3–6.4/2.1	4 @ 5.5 GH	2
(*Khan et al.*, 2021)	2.98 × 1.31	5.6–5.67/0.07	12 @ 5.6 GHz	4
This work	0.7 × 0.7	3.8–6/2.2	4.8 @ 4.2 GHz	4
		3.2–6/2.2	6.7 @ 3.9	4

9. Conclusion

The design of a novel 2 × 2 element FSS based MIMO antenna array is verified practically to be suitable for sub-6 GHz wireless communication applications. The circular ring-shaped radiating elements of the MIMO antenna are orthogonally arranged to realize high isolation (>15 dB) between the different antenna elements over 3.5–6 GHz. This arrangement helps improve the performance of the MIMO system by reducing interference and enhancing signal quality. Orthogonal placement of the radiating elements provides spatial diversity, where the radiating elements receive independent multipath signals due to their spatial separation. This diversity improves the system's resilience to fading and enhances its ability to recover from signal degradation caused by fading or obstructions. The high isolation achieved through orthogonal placement enables better utilization of the available channel capacity. By reducing interference and improving signal quality, the FSS based MIMO antenna array can achieve higher data rates and increased overall capacity. Moreover, it is shown that by locating the proposed FSS above the antenna at a certain height the gain of the antenna can be increased over a wide bandwidth from 3 to 6 GHz.

Conflict of Interest

The authors declare no conflicts of interest relevant to this study.

Data Availability Statement

Data were not used, nor created for this research.

Acknowledgments
Dr. Mohammad Alibakhshikenari acknowledges support from the CONEX-Plus programme funded by Universidad Carlos III de Madrid and the European Union's Horizon 2020 research and innovation programme under the Marie Sklodowska-Curie grant agreement No. 801538. The authors also sincerely appreciate funding from Researchers Supporting Project number (RSPD2023R699), King Saud University, Riyadh, Saudi Arabia. Besides above, the Article Processing Charge (APC) was afforded by Universidad Carlos III de Madrid (Agreement CRUE-Madroño 2023). All of the figures, materials, and data within the manuscript are original and owned by authors.

References

Akram, M. R., Bai, X., Jin, R., Vandenbosch, G. A. E., Premaratne, M., & Zhu, W. (2019). Photon spin Hall effect-based ultra-thin transmissive metasurface for efficient generation of OAM waves. *IEEE Transactions on Antennas and Propagation*, *67*(7), 4650–4658. https://doi.org/10.1109/tap.2019.2905777

Akram, M. R., Mehmood, M. Q., Bai, X., Jin, R., Premaratne, M., & Zhu, W. (2019). High efficiency ultrathin transmissive metasurfaces. *Advanced Optical Materials*, *7*(11), 1801628. https://doi.org/10.1002/adom.201801628

Arpan, D., Upadhyaya, T., Patel, J., Patel, R., & Palandoken, M. (2020). Flexible CPW fed transparent antenna for WLAN and sub-6 GHz 5G applications. *Microwave and Optical Technology Letters*, *62*(5), 2090–2103. https://doi.org/10.1002/mop.32287

Aw, M. S., Ashwath, K., Tanweer, A., & Ali, T. (2019). A compact two element MIMO antenna with improved isolation for wireless applications. *Journal of Instrumentation*, *14*(06), P06014. https://doi.org/10.1088/1748-0221/14/06/p06014

Basar, E., Di Renzo, M., De Rosny, J., Debbah, M., Alouini, M. S., & Zhang, R. (2019). Wireless communications through reconfigurable intelligent surfaces. *IEEE Access*, *7*, 116753–116773. https://doi.org/10.1109/access.2019.2935192

Biswas, A. K., & Chakraborty, U. (2019). Reduced mutual coupling of compact MIMO antenna designed for WLAN and WiMAX applications. *International Journal of RF and Microwave Computer-Aided Engineering*, *29*(3), e21629. https://doi.org/10.1002/mmce.21629

Chouhan, S., & Malviya, L. (2020). Four-port shared rectangular radiator with defected ground for wireless application. *International Journal of Communication Systems*, *33*(9), e4356. https://doi.org/10.1002/dac.4356

Dabas, T., Gangwar, D., Kumar, B. K., & Gautam, A. K. (2018). Mutual coupling reduction between elements of UWB MIMO antenna using small size uniplanar EBG exhibiting multiple stop bands. *International Journal of Electronics and Communications*, *93*, 32–38. https://doi.org/10.1016/j.aeue.2018.05.033

Deng, Y. J., Li, J., Zhao, L., & Guo, L. (2017). A dual-band inverted-F MIMO antenna with enhanced isolation for WLAN applications. *IEEE Antennas and Wireless Propagation Letters*, *16*, 2270–2273. https://doi.org/10.1109/lawp.2017.2713986

Desai, A., Bui, C. D., Patel, J., Upadhyaya, T., Byun, G., & Nguyen, T. K. (2020). Compact wideband four element optically transparent MIMO antenna for mm-wave 5G applications. *IEEE Access*, *8*, 194206–194217. https://doi.org/10.1109/access.2020.3033314

Desai, A., Upadhyaya, T., Patel, J., Patel, R., & Palandoken, M. (2020). Flexible CPW fed transparent antenna for WLAN and sub-6 GHz 5G applications. *Microwave and Optical Technology Letters*, *62*(5), 2090–2103. https://doi.org/10.1002/mop.32287

Din, I. U., Kiyani, A., Naqvi, S. I., Al-Gburi, A. J. A., Abbas, S. M., & Ullah, S. (2022). A low-cost wideband MIMO antenna for IoT applications. In *IEEE International Symposium on Antennas and Propagation and USNC-URSI Radio Science Meeting (AP-S/URSI)* (pp. 2064–2065).

Din, I. U., Ullah, S., Naqvi, S. I., Ullah, R., Ullah, S., Ali, E. M., & Alibakhshikenari, M. (2022). Improvement in the gain of UWB antenna for GPR applications by using frequency-selective surface. *International Journal of Antennas and Propagation*, *2022*, 1–12. https://doi.org/10.1155/2022/2002552

Din, U., Abbasi, U., Shihzad, K., & Jayakody (2023). A novel compact ultra-wideband frequency-selective surface-based antenna for gain enhancement applications. *Journal of Electromagnetic Engineering and Science*, *23*(2), 108–121.

Dong, J., Yu, X., & Deng, L. (2017). A decoupled multiband dual-antenna system for WWAN/LTE smartphone applications. *IEEE Antennas and Wireless Propagation Letters*, *16*, 1528–1532. https://doi.org/10.1109/lawp.2017.2647807

El Mossallamy, M. A., Zhang, H., Song, L., Seddik, K. G., & Han, Z. (2020). Reconfigurable intelligent surfaces for wireless communications: Principles, challenges, and opportunities. *IEEE Transactions on Cognitive Communications and Networking*, *6*(3), 990–1002. https://doi.org/10.1109/tccn.2020.2992604

Farahani, H. S., Veysi, M., Kamyab, M., & Tadjalli, A. (2010). Mutual coupling reduction in patch antenna array using a UC-EBG superstrate. *IEEE Antennas and Wireless Propagation Letters*, *9*, 57–59. https://doi.org/10.1109/lawp.2010.2042565

Fathima, N., Nayana, K. S., Ali, T., & Biradar, R. C. (2017). A miniaturized slotted ground fractal Koch multiband antenna for wireless applications. In *2nd IEEE International Conference on Recent Trends in Electronics* (pp. 251–255). Information & Communication Technology (RTEICT).

Gupta, A., & Jha, R. K. (2015). Survey of 5G network: Architecture and emerging technologies. *IEEE Access*, *3*, 1206–1232. https://doi.org/10.1109/access.2015.2461602

Hussain, N., Jeong, M., Park, J., & Kim, N. (2019). A broadband circularly polarized fabry-perot resonant antenna using a single-layered PRS for 5G MIMO applications. *IEEE Access*, *7*, 42897–42907. https://doi.org/10.1109/access.2019.2908441

Iqbal, A., Saraereh, O. A., Ahmad, A. W., & Bashir, S. (2017). Mutual coupling reduction using F-shaped stubs in UWB-MIMO antenna. *IEEE Access*, *6*, 2755–2759. https://doi.org/10.1109/access.2017.2785232

Jehangir, S. S., Sharawi, M. S., & Shamim, A. (2018). Highly miniaturized semi-loop meandered dual-band MIMO antenna system. *IET Microwaves, Antennas & Propagation*, *12*(6), 864–871. https://doi.org/10.1049/iet-map.2017.0701

Khalid, I. N., Hussain, R., Fawad, M., Amin, Y., Fawad, Mirjavadi, S. S., et al. (2020). 4-Port MIMO antenna with defected ground structure for 5G millimeter wave applications. *Electronics*, *9*(1), 71. https://doi.org/10.3390/electronics9010071

Khan, J., Ullah, S., Tahir, F. A., Tubbal, F., & Raad, R. (2021). A Sub-6 GHz MIMO antenna array for 5G wireless Terminals. *Electronics*, *10*(24), 3062. https://doi.org/10.3390/electronics10243062

Kundu, L. (2016). Information theoretic limits on MIMO antennas. Ph.D. Thesis. North Carolina State University.

Lee, C. H., Chen, S. Y., & Hsu, P. (2009). Integrated dual planar inverted F antenna with enhanced isolation. *IEEE Antennas and Wireless Propagation Letters*, *8*, 963–965. https://doi.org/10.1109/lawp.2009.2029707

Lin, I. K. C., Jamaluddin, M. H., Awang, A., Selvaraju, R., Dahri, M. H., Yen, L. C., & Rahim, H. A. (2019). A triple band hybrid MIMO rectangular dielectric resonator antenna for LTE applications. *IEEE Access*, *7*, 122900–122913. https://doi.org/10.1109/access.2019.2937987

Luo, C.-M., Hong, J.-S., & Zhong, L.-L. (2015). Isolation enhancement of a very compact UWB-MIMO slot antenna with two defected ground structures. *IEEE Antennas and Wireless Propagation Letters*, *14*, 1766–1769. https://doi.org/10.1109/lawp.2015.2423318

Madhav, B. T., Usha Devi, Y., & Anilkumar, T. (2019). Defected ground structured compact MIMO antenna with low mutual coupling for automotive communications. *Microwave and Optical Technology Letters*, *61*(3), 794–800. https://doi.org/10.1002/mop.31626

Malviya, L., & Chouhan, S. (2019). Multi-cut four-port shared radiator with stepped ground and diversity effects for WLAN application. *International Journal of Microwave and Wireless Technologies*, *11*(10), 1044–1053. https://doi.org/10.1017/s1759078719000680

Ove, E., & Johansson, A. J. (2011). Is orbital angular momentum (OAM) based radio communication an unexploited area. *IEEE Transactions on Antennas and Propagation*, *60*(2), 1126–1131.

Pandit, S., Mohan, A., & Ray, P. (2018). A compact four-element MIMO antenna for WLAN applications. *Microwave and Optical Technology Letters*, *60*(2), 289–295. https://doi.org/10.1002/mop.30961

Qian, K.-W., Huang, G.-L., Liang, J.-J., Qian, B., & Yuan, T. (2018). An LTCC interference cancellation device for closely spaced antennas decoupling. *IEEE Access*, *6*, 68255–68262. https://doi.org/10.1109/access.2018.2879569

Rappaport, T. S., Sun, S., Mayzus, R., Zhao, H., Azar, Y., Wang, K., et al. (2013). Millimeter wave mobile communications for 5G cellular: It will work!. *IEEE Access*, *1*, 335–349. https://doi.org/10.1109/access.2013.2260813

Roy, S., Ghosh, S., & Chakarborty, U. (2019). Compact dual wide-band four/eight elements MIMO antenna for WLAN applications. *International Journal of RF and Microwave Computer-Aided Engineering*, *29*(7), e21749. https://doi.org/10.1002/mmce.21749

Saadh, M. A., Ashwath, K., Ramaswamy, P., Ali, T., & Anguera, J. (2020). A uniquely shaped MIMO antenna on FR4 material to enhance isolation and bandwidth for wireless applications. *AEU-International Journal of Electronics and Communications*, *123*, 15331.

Saxena, S., Kanaujia, B. K., Dwari, S., Kumar, S., & Tiwari, R. (2018). MIMO antenna with built-in circular shaped isolator for sub-6 GHz 5G applications. *Electronics Letters*, *54*(8), 478–480. https://doi.org/10.1049/el.2017.4514

Sharma, S. K., & Wang, A. (2018). Two elements MIMO antenna for tablet size ground plane with reconfigurable lower bands and consistent high band radiating elements. In *IEEE International Symposium on Antennas and Propagation & USNC/URSI National Radio Science Meeting* (pp. 25–26).

Shoaib, S., Shoaib, I., Shoaib, N., Chen, X., & Parini, C. G. (2014). Design and performance study of a dual element multiband printed monopole antenna array for MIMO terminals. *IEEE Antennas and Wireless Propagation Letters*, *13*, 329–332. https://doi.org/10.1109/lawp.2014.2305798

Ushikoshi, D., Higashiura, R., Tachi, K., Fathnan, A. A., Mahmood, S., Takeshita, H., et al. (2023). Pulse-driven self-reconfigurable meta-antennas. *Nature Communications*, *14*(1), 633. https://doi.org/10.1038/s41467-023-36342-1

Venkateswara Rao, M., Madhav, B. T., Krishna, J., Usha Devi, Y., Anilkumar, T., & Nadh, P. (2019). CSRR-loaded T-shaped MIMO antenna for 5G cellular networks and vehicular communications. *International Journal of RF and Microwave Computer-Aided Engineering*, *29*(8), e21799. https://doi.org/10.1002/mmce.21799